



## UvA-DARE (Digital Academic Repository)

### Glow with the flow: Quantifying blood flow and photoluminescence signal in biological tissue

Nadort, A.

**Publication date**

2015

**Document Version**

Final published version

[Link to publication](#)

**Citation for published version (APA):**

Nadort, A. (2015). *Glow with the flow: Quantifying blood flow and photoluminescence signal in biological tissue*. [Thesis, fully internal, Universiteit van Amsterdam].

**General rights**

It is not permitted to download or to forward/distribute the text or part of it without the consent of the author(s) and/or copyright holder(s), other than for strictly personal, individual use, unless the work is under an open content license (like Creative Commons).

**Disclaimer/Complaints regulations**

If you believe that digital publication of certain material infringes any of your rights or (privacy) interests, please let the Library know, stating your reasons. In case of a legitimate complaint, the Library will make the material inaccessible and/or remove it from the website. Please Ask the Library: <https://uba.uva.nl/en/contact>, or a letter to: Library of the University of Amsterdam, Secretariat, P.O. Box 19185, 1000 GD Amsterdam, The Netherlands. You will be contacted as soon as possible.



5

---

UPCONVERSION NANOPARTICLES

---

Parts in this chapter are adapted from co-authored publications:

Ref. 9.

A. V. Zvyagin, Z. Song, **A. Nadort**, V. K. A. Sreenivasan, and S. M. Deyev, "Luminescent Nanomaterials for Molecular-Specific Cellular Imaging," in Handbook of Nano-Optics and Nanophotonics (Springer, 2013), pp. 563-596.

Ref. 12

Z. Song, Y. G. Anissimov, J. Zhao, A. V. Nechaev, **A. Nadort**, D. Jin, T. W. Prow, M. S. Roberts, and A. V. Zvyagin, "Background free imaging of upconversion nanoparticle distribution in human skin," Journal of biomedical optics 18, 061215-061215 (2013).

Ref. 34

K. Liu, J. A. Holz, Y. Ding, X. Liu, Y. Zhang, T. Langping, X. Kong, B. Priem, **A. Nadort**, S. A. G. Lambrechts, M. C. G. Aalders, W. J. Buma, P. D. Y. Liu, and H. Zhang, "Targeted labeling of early-stage tumor spheroid in chorioallantoic membrane model with upconversion nanoparticles," Nanoscale (2014).

Ref. 36

A. E. Guller, A. N. Generalova, E.V. Petersen, A.V. Nechaev, I.A. Trusova, N.N. Landyshev, **A. Nadort**, E.A. Grebenik, S.M. Deyev, A.B. Shekhter and A.V. Zvyagin, "Cytotoxicity and non-specific cellular uptake of bare and surface-modified upconversion nanoparticles in human skin cells," Nano Research (2014).

**ABSTRACT** This chapter introduces optical techniques to assess biological tissues based on photoluminescent probes, as well as the relevant tissue optical properties and the desirable characteristics of the luminophores. Upconversion nanoparticles represent a class of luminophores that are particularly interesting for molecular imaging in the biomedical context. Therefore, their optical properties, the upconversion process and an introduction on bioconjugation of these nanomaterials is included.

## 5.1 INTRODUCTION

The results of the previous chapters on laser speckle flowmetry are promising for functional monitoring of the microvasculature in the clinic. As elucidated in Chapter 1, the microcirculation plays an important role in tumour development but can also be effective in tumour therapy and delivery of drugs and contrast agents, for example mediated by the enhanced permeability and retention (EPR) effect and targeted delivery. Although the EPR effect and its applicability in tumour detection and therapy were described almost 30 years ago [1], therapies exploiting the tumour vessel hyperpermeability are still limited in clinical use and need further investigations [2, 3]. Underlying this apparently moderate progress is the complexity of tumour development, in particular the structural features and biochemical processes, which can vary both spatially and temporally within one tumour but also between tumour types, location and patient specific characteristics [4, 5]. Therefore, imaging the tumour microvasculature is instrumental but not sufficient for a thorough understanding of tumour development. In addition, tumour detection by increased microvasculature is only possible in case of hyper-vascularised tumours, which are characteristic for advanced stages of cancer and imply reduced patient survival [6]. Therefore, more sensitive detection approaches at the early stages of cancer are needed.

The increased focus on nanotechnology in cancer research can potentially accelerate the progress in tumour detection and therapy [7]. Controlling the size, shape and surface properties of nanoparticles allows controlling their interaction with normal versus cancer cells and tissue [2]. Therefore, nano-engineering can provide solutions for cancer therapy. Visualizing the interaction of nanoparticles with tumour vasculature or tumour cells is an important capability for cancer research, where a high imaging contrast is essential. In this chapter, I will discuss the desirable characteristics of nanoparticles that result in a high imaging contrast and introduce a novel class of nanoparticles, called upconversion nanoparticles (UCNPs), as promising photoluminescent nanomaterials.

## 5.2 PHOTOLUMINESCENT IMAGING OF BIOTISSUE

The ideal luminophore for biomedical imaging has excellent optical properties, as well as chemical and physical stability in biological environments [8, 9]. These optical properties include a high absorption coefficient and quantum yield for brightness, a large Stokes shift for minimal interference between excitation and emission light, and preferably no photoluminescence intermittency (blinking) and irreversible light-induced transitions to the dark states (photobleaching). In addition, the excitation and emission radiation should substantially penetrate into biological tissue. This last property is determined by the optical absorption and scattering properties of biological tissue, where the absorption is mainly due to the three tissue constituents water, oxygenated and deoxygenated haemoglobin. In Fig. 5.1 a the absorption due to blood and water in skin tissue is plotted for the visible (VIS) and near infrared (NIR) wavelength range. In skin the pigment melanin is also responsible for absorption of light, although this is highly dependent on skin type (e.g. Caucasian, Mediterranean, Negroid) [10] and therefore excluded from this graph. For Caucasian skin the absorption by melanin (0.4%) is less than the absorption by blood for wavelengths >400 nm [11]. The total effective attenuation coefficient in skin including the effects of scattering

is also calculated and plotted [12]. In Fig. 5.1b the tissue penetration depth of light in skin is visualized for the UV-VIS-NIR spectrum. The tissue transparency window (650 - 1300 nm) is marked by the low effective attenuation and deep tissue penetration depth of light. Luminophores whose excitation and emission fall in this window can be detected at greater depths in tissue. In addition, unwanted tissue autofluorescence is much lower compared to exciting in the shorter wavelength range.

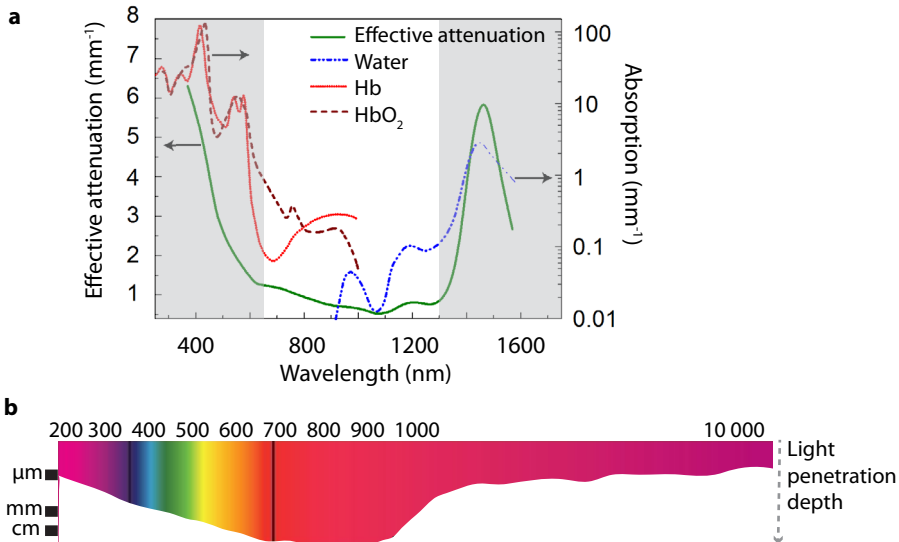


**Figure 5.1 | Optical properties of skin.** (a) Optical effective attenuation spectrum of skin (green solid line), dominated by absorption spectra of water (blue -.-), deoxygenized haemoglobin (Hb, brown - -), oxygenized haemoglobin (HbO<sub>2</sub>, red solid) and scattering of skin. The biological tissue transparency window is the unshaded area (650 - 1300 nm). Adapted from ref. [12]. (b) Light penetration depth in skin tissue for the UV-VIS-NIR wavelength range, calculated as the depth where 37% of the incident light ( $e^{-1} = 0.37$ ) is not diffused or absorbed.

Near infrared dyes are a group of organic fluorescent dyes whose excitation and emission properties fall in the tissue transparency window and are therefore attractive for cancer targeting and imaging [8, 13]. However, conventional NIR dyes have a poor hydrophilicity and stability in biological media, a low quantum yield and low photostability due to bleaching, although recent developments of NIR dyes have improved these characteristics to some extent [8, 14]. An alternative way to use NIR excitation light is the use of 2-photon imaging where luminophores absorb two NIR photons simultaneously and subsequently emit one photon of higher energy (shorter wavelength) than each of the excitation photons [15, 16]. This technique has delivered high-quality images and has optical sectioning capability enabling tomography. However, the chance for the simultaneous absorption of two photons is low and excitation intensities of the order  $10^6$  -  $10^9$  W/cm<sup>2</sup> are needed for sufficient signal detection [16], acquired with expensive short pulsed lasers. Yet another process that involves the generation of anti-Stokes shifted light is photon upconversion, based on the sequential absorption and energy transfer steps involving real metastable states of the luminophore as detailed in the next section. This process occurs at excitation intensities of  $1$  -  $10^3$  W/cm<sup>2</sup> [17], attainable with low-cost continuous-wave lasers. Similar to dynamic light scattering techniques, the utility and production of upconversion materials

depended highly on the introduction of the laser more than 50 years ago [17, 18]. However, the synthesis of nanosized upconversion materials that can be dispersed in a solution was a challenging task, which was achieved only ten years ago in the early 2000's. [19, 20]. Since then, the application of upconversion nanoparticles (UCNPs) in the biomedical sciences expanded majorly due to their key photophysical advantages: excitation in the NIR and emission in the VIS/NIR region at modest excitation intensity also characterised by a long emission lifetimes ( $\sim$ milliseconds) compared to conventional fluorophores ( $\sim$ nanoseconds). There are no endogenous molecules known that are capable of this conversion, therefore emission of UCNPs can be discriminated from that of autofluorescence, leading to strong suppression of the background, as for example is shown in Fig. 5.2. In addition, the long lifetimes allow for time-gated detection, which can eliminate the residual background signals due to the excitation beam and autofluorescence. UCNPs have other advantageous optical properties such as nonblinking, nonphotobleaching, sharp emission bands and a large anti-Stokes shift [21].

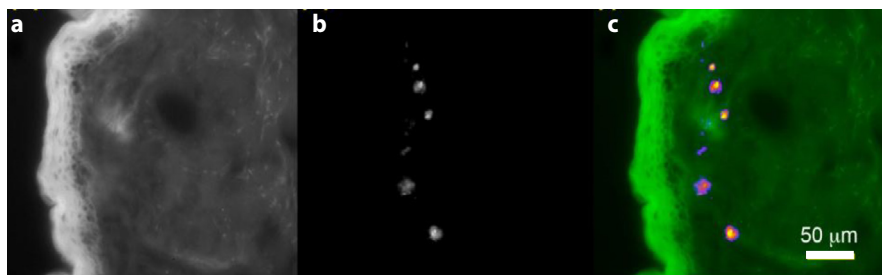


**Figure 5.2.** | UCNPs ( $\text{NaYF}_4\text{:Yb,Tm}$ ) distribution in excised skin. (a) UV (365 nm) excited autofluorescence image of skin tissue slice treated with UCNPs (b) NIR (980 nm) excited upconversion image of same skin tissue slice showing only UCNPs signal and no background of autofluorescence and (c) pseudo-colour overlay of (a) and (b) showing UCNPs (purple) in skin furrow and dermis (green), respectively. Adapted from ref. [12].

### 5.3 THE UPCONVERSION PROCESS

UCNPs are dopant-host systems where trivalent lanthanide ions are dispersed in an inorganic nanocrystal matrix. The lanthanide ions are optically active centres, which can absorb photons and emit photoluminescence. Generally, the photoluminescence arises from electronic transitions in the 4f-4f orbital within a single lanthanide ion. The 4f electrons are shielded by the complete outer 5s and 5p shells resulting in sharp emission bands. The electronic transmission within the 4f shell are forbidden by quantum mechanical selection rules, but can happen due to local crystal field-induced relaxation, resulting in long lifetimes of the higher energy levels of the 4f electrons ( $\sim$  milliseconds). This metastable excited state enables the occurrence of sequential excitation to a second energy level, and the exchange of energy by ion-ion interactions [17, 21]. There are five basic mechanisms for upconversion identified: excited-state absorption, energy transfer upconversion, cooperative sensitization upconversion, cross relaxation and photon avalanche [21, 22].

Most photoluminescence by UCNPs relies on the energy transfer upconversion process, which is schematically shown in Figs. 5.3 and 5.4. A detailed energy diagram of the transitions in two often used dopant pairs, Ytterbium ( $\text{Yb}^{3+}$ ) - Erbium ( $\text{Er}^{3+}$ ) and Ytterbium - Thulium

um ( $\text{Tm}^{3+}$ ), is shown in Fig. 5.3a [9]. A two-level  $\text{Yb}^{3+}$  ion serves as the donor (also known as the sensitizer) which has a high absorption cross-section for the NIR excitation photons via the  ${}^2\text{F}_{7/2} \rightarrow {}^2\text{F}_{5/2}$  transition path. Then, it non-radiatively transfers the excitation energy to a neighbouring  $\text{Yb}^{3+}$  ion, or a neighbouring  $\text{Er}^{3+}$  (or  $\text{Tm}^{3+}$ ) ion (also known as the activator). As a result, the ensemble of the excited  $\text{Yb}^{3+}$  ions forms a delocalised quasi-exciton across the entire nanocrystal matrix maintained by the non-radiative energy exchange process. This excitation energy is continuously transferred to the network of activators,  $\text{Er}^{3+}$  or  $\text{Tm}^{3+}$ , a fast process at a rate of  $1000 \text{ s}^{-1}$  for the representative crystal matrix  $\text{Cs}_3\text{Lu}_2\text{Br}_9$  [23]. The activated ion, for example,  $\text{Er}^{3+}$  in the  ${}^4\text{I}_{11/2}$  metastable state can coalesce with the metastable  $\text{Yb}^{3+}$  ( ${}^2\text{F}_{5/2}$ ) via the collective pair-wise process called energy transfer upconversion. As a result, the  $\text{Er}^{3+}$  ( ${}^4\text{I}_{11/2}$ ) makes a transition to the next-level excited state  $\text{Er}^{3+}$  ( ${}^4\text{F}_{7/2}$ ), followed by a rapid non-radiative transition to  $\text{Er}^{3+}$  ( ${}^4\text{S}_{3/2}$ ) at the expense of the  $\text{Yb}^{3+}$  ( ${}^2\text{F}_{5/2}$ )  $\rightarrow \text{Yb}^{3+}$  ( ${}^2\text{F}_{7/2}$ ) falling back to the ground state. The  $\text{Er}^{3+}$  ( ${}^4\text{S}_{3/2}$ ) emits in a multiplet green spectral band, and also in a multiplet red spectral band, following the non-radiative phonon-assisted transition  $\text{Er}^{3+}$  ( ${}^4\text{S}_{3/2}$ )  $\rightarrow \text{Er}^{3+}$  ( ${}^4\text{F}_{9/2}$ ), as one can see in the emission spectral bands in Fig. 5.3b. The  $\text{Er}^{3+}$  ( ${}^4\text{F}_{9/2}$ ) population is also built up via an alternative excitation path: non-radiative transition  $\text{Er}^{3+}$  ( ${}^4\text{I}_{11/2}$ )  $\rightarrow \text{Er}^{3+}$  ( ${}^4\text{I}_{13/2}$ ), followed by the energy transfer upconversion  $\text{Er}^{3+}$  ( ${}^4\text{I}_{13/2}$ )  $\rightarrow \text{Er}^{3+}$  ( ${}^4\text{F}_{9/2}$ ) and  $\text{Yb}^{3+}$  ( ${}^2\text{F}_{5/2}$ )  $\rightarrow \text{Yb}^{3+}$  ( ${}^2\text{F}_{7/2}$ ) back to the ground state. Other energy transfer paths involve the absorption and exchange of 3 excitation photons resulting in a blue emission band (Fig. 5.3b). The energy diagram of the  $\text{Tm}^{3+}$  activator ion results in two main emission bands at the NIR and blue wavelengths (Fig. 5.3c).

Fig. 5.4 presents a simplified schematic diagram of energy transfer upconversion. At low (sub-saturation,  $\sim 100 \text{ W/cm}^2$ ) excitation intensity  $I_{\text{ex}}$  the emitted upconversion signal depends on the population of the second energy level which depends on  $I_{\text{ex}}^2$  for a 2-photon process, generally  $I_{\text{ex}}^n$  for an  $n$ -photon process (although competitive energy transfer processes and size-dependent nonradiative decay result in a value somewhat deviating from  $n$  [24-27]). Due to this nonlinearity, the upconversion efficiency  $\eta_{\text{uc}}$  decreases when  $I_{\text{ex}}$  decreases. This poses a challenge to tissue imaging, since tissue scattering decreases  $I_{\text{ex}}$  with imaging depth resulting in a quick reduction of the photoluminescence signal with depth. A relatively high upconversion efficiency is observed for the Yb,Er and Yb,Tm dopant pairs in a host matrix consisting of  $\text{NaYF}_4$  [25], typically around 1% for nanosized materials [28]. The  $\eta_{\text{uc}}$  also depends on the synthesized crystal purity, phase and size and is therefore an important parameter to measure for feedback on the design and synthesis of UCNPs. In Chapter 6 a quantitative measurement system for the determination of the absolute  $\eta_{\text{uc}}$  is designed using an integrating sphere set up. Since the background signal is virtually absent detection of UCNPs with a high contrast is achievable in spite of the low  $\eta_{\text{uc}}$ . In Chapter 6 the UCNP imaging limits are explored both experimentally and theoretically by imaging of a single particle in the context of biological tissue. Besides the assessment of optical properties and imaging systems, for UCNP-based biomedical applications biocompatible particles are required to uncover information about living cells en tissues.

## 5.4 BIOCONJUGATION

Generally, living systems treat exogenous material as an unwelcome intruder and engage in disposal protocols. For a more meaningful communication with cells, an ideal optically

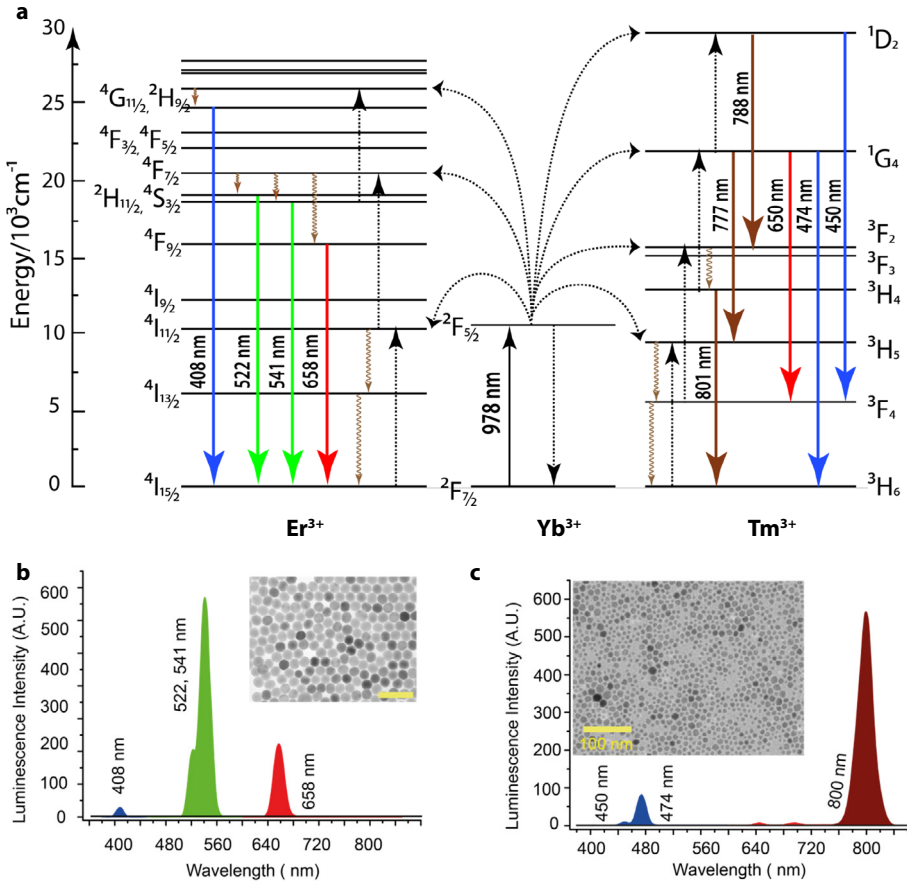


**Figure 5.3 | Energy levels in photon upconversion.** (a) Schematic energy level diagram of  $\text{Yb}^{3+}$  sensitizer ions with participating Erbium ( $\text{Er}^{3+}$ ) or Thulium ( $\text{Tm}^{3+}$ ) activator ions. The upconversion process results in specific emission spectra for  $\text{NaYF}_4:\text{Yb,Er}$  (b) and  $\text{NaYF}_4:\text{Yb,Tm}$  (c) nanomaterials. The insets show their corresponding transmission electron microscopy images. Adapted from ref. [12] and ref. [9].

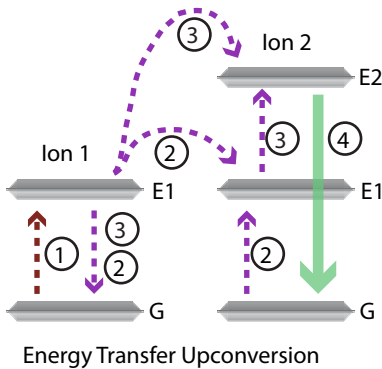


**Figure 5.4 | Schematic diagram of energy transfer upconversion process in UCNPs.** The following consecutive steps can be identified: 1. photon excitation of ion 1 to energy level E1; 2. energy transfer to energy level E1 (ion 2) and remission to ground state G (ion 1); 3. energy transfer to energy level E2 (ion 3) and remission to ground state G (ion 1) and 4. emission of one higher energy photon and remission to ground state G (ion 2).

bright luminophore exhibits excellent biochemical properties, such as a good dispersibility in buffers and suitable chemical functionality allowing strong attachment of biomolecules – a process termed bioconjugation. Bioconjugation is a critical step in building biomolecular nanoparticle assemblies, serving two main functions in the context of cancer research: facilitating prolonged circulation times in the bloodstream and tumour targeting purposes.

The biochemical properties of UCNP provide a challenge in this regard. Firstly, as-synthesized UCNP are hydrophobic due to surface oleic groups and would rapidly aggregate when dispersed in water or buffer, making them useless for further biomedical interactions. Secondly, the most popular inorganic host of UCNP,  $\text{NaYF}_4$  does not provide adequate surface anchoring points for firm docking of biomolecules. And thirdly, the  $\eta_{uc}$  is highly susceptible to surface functionalization, where high-energy vibronic modes of some functional groups provide non-radiative depletion of the excited states of the activator ions [29]. A common solution is to cover the surface of nanoparticles by polyethylene-glycol (PEG). These groups prevent nanoparticle merging and aggregation via the mechanism of steric hindrance [30]. Also, PEGylation represents the core of the so-called stealth functionalization preventing PEGylated nanoparticles intravenously injected into the blood stream from rapid immune-mediated removal [31]. However, PEG groups have their disadvantages associated with poorly-controlled polymer chains, and PEG chemistry is expensive [9]. Another methodology to improve the UCNP surface anchoring properties is to coat the particles with an additional layer that is suitable for subsequent bioconjugation. Coating the UCNP with a silica shell represents an attractive approach due to the shell stability in the biological range of pH, and maturity of the silica surface coating technology [32]. A different coating method makes use of amphiphilic polymers that represent molecules with hydrophobic and hydrophilic terminals. This approach has been successfully demonstrated for the surface activation of several inorganic nanocrystals [33]. An amphiphilic polymer can intercalate the hydrophobic surface groups with their hydrophobic portion and their extending hydrophilic portion ensures water solubility. Addition of bis(6-aminohexyl)amine resulted in cross-linking of the polymer chains around each nanoparticle and a successful and robust transfer of hydrophobically capped nanocrystals from organic to aqueous solution [33]. Suitable amphiphilic polymers for UCNP are for example poly(maleic anhydride-alt-1-octadecene) (UCNP-PMAO), polyethylenimine (UCNP-PEI), poly(D,L-lactide) (UCNP-PLA), and poly(lactide-co-glycolide) (UCNP-PLG). A layer-by-layer approach can be applied to control the coating thickness. These surface modifications are illustrated in Fig. 5.5. An additional advantage of the amphiphilic polymer coating is the shielding of the surface from environmental interaction to prevent quenching processes. In Chapter 7, the amphiphilic polymer coating is successfully applied to UCNP, showing prolonged stability in water and buffer solutions. A last modification strategy is based on ligand exchange, where surface oleates are first removed to obtain ligand-free UCNP, which are subsequently treated with hydrophilic surface groups such as poly acrylic acid (UCNP-PAA) making them water soluble (referred to in Chapter 8 [34]).

Amphiphilic polymer coated UCNP with exposed COOH functional groups are suitable for further functionalization. Using a universal bioconjugation protocol, i.e. EDC/sNHS reaction, subsequent attachment of proteins (e.g. antibodies), or applying the modular approach using streptavidin:biotin or barstar:barnase protocols is straightforward [35].

In Chapter 7, this latter protocol is utilized to biofunctionalize UCNPs with antibodies targeting human breast cancer. This shows that UCNPs not only possess unique optical advantages for imaging in living tissues, they also serve as a docking platform that can be engineered for targeted detection and imaging of tumours.

In the next chapters, UCNP photophysical and biochemical properties are put to the experimental test, specifically imaging of single UCNPs (Chapter 6) and the detection of a small cluster of UCNP-targeted breast cancer cells (Chapter 7). In both chapters, the results are interpreted in the theoretical framework of UCNP detection in tissue, which allows projection onto imaging scenarios using UCNPs and predict their performance. This helps to identify feasible applications of UCNPs in the biomedical context.

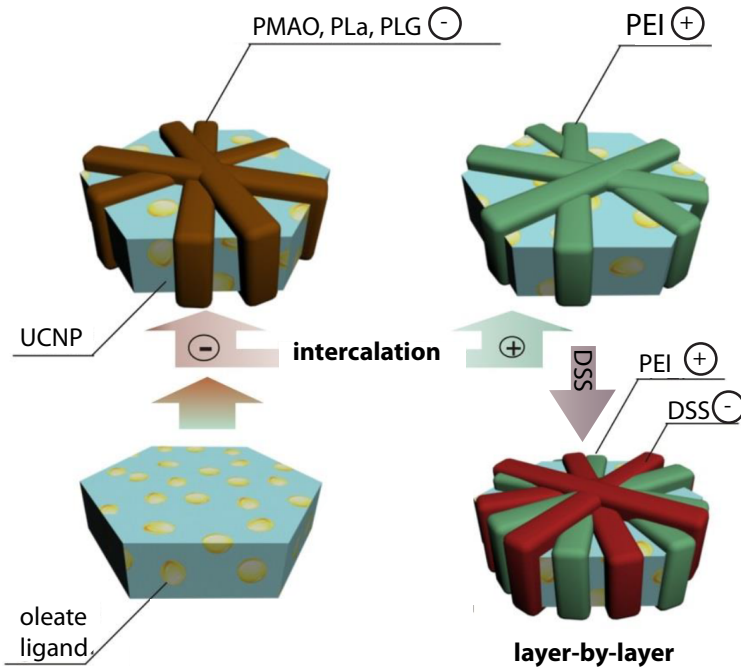


**Figure 5.5 | Surface modification of UCNPs.** As-synthesized UCNP ( $\text{NaYF}_4:\text{Yb,Er}$ ) surface modified with amphiphilic polymers (negatively-charged PMAO, PLa and PLG; and positively-charged PEI) performed by intercalation. The resultant particles were colloiddally stable UCNP-PMAO, UCNP-PLa, UCNP-PLG (negative) and UCNP-PEI (positive). Bilayer modification of UCNP-PEI with DSS was performed by the layer-by-layer assembly method and resulted in UCNP-PEI-DSS. Adapted from ref. [36]

## 5.5 REFERENCES

1. Y. Matsumura and H. Maeda, "A new concept for macromolecular therapeutics in cancer chemotherapy: mechanism of tumorotropic accumulation of proteins and the antitumor agent smancs," *Cancer Res.* **46**, 6387-6392 (1986).
2. S. D. Perrault, C. Walkey, T. Jennings, H. C. Fischer, and W. C. Chan, "Mediating tumor targeting efficiency of nanoparticles through design," *Nano Lett.* **9**, 1909-1915 (2009).
3. A. Z. Wang, R. Langer, and O. C. Farokhzad, "Nanoparticle delivery of cancer drugs," *Annu. Rev. Med.* **63**, 185-198 (2012).
4. P. Carmeliet and R. K. Jain, "Angiogenesis in cancer and other diseases," *Nature* **407**, 249-257 (2000).
5. U. Prabhakar, H. Maeda, R. K. Jain, E. M. Sevick-Muraca, W. Zamboni, O. C. Farokhzad, S. T. Barry, A. Gabizon, P. Grodzinski, and D. C. Blakey, "Challenges and key considerations of the enhanced permeability and retention effect for nanomedicine drug delivery in oncology," *Cancer Res.* **73**, 2412-2417 (2013).
6. M. Sant, T. Aareleid, F. Berrino, M. B. Lasota, P. Carli, J. Faivre, P. Grosclaude, G. Hedelin, T. Matsuda, and H. Møller, "EUROCORE-3: survival of cancer patients diagnosed 1990-94—results and commentary," *Ann. Oncol.* **14**, v61-v118 (2003).
7. M. Wang and M. Thanou, "Targeting nanoparticles to cancer," *Pharmacol. Res.* **62**, 90-99 (2010).
8. S. Luo, E. Zhang, Y. Su, T. Cheng, and C. Shi, "A review of NIR dyes in cancer targeting and imaging," *Biomaterials* **32**, 7127-7138 (2011).
9. A. V. Zvyagin, Z. Song, A. Nadort, V. K. A. Sreenivasan, and S. M. Deyev, "Luminescent Nanomaterials for Molecular-Specific Cellular Imaging," in *Handbook of Nano-Optics and Nanophotonics* (Springer, 2013), pp. 563-596.
10. N. Bosschaart, R. Mentink, J. H. Kok, T. G. Van Leeuwen, and M. C. Aalders, "Optical properties of neonatal skin measured *in vivo* as a function of age and skin pigmentation," *J. Biomed. Opt.* **16**, 097003-097003-097010 (2011).
11. N. Bosschaart, "Quantitative and localized spectroscopy for non-invasive bilirubinometry in neonates," (University of Amsterdam, Amsterdam, 2012).
12. Z. Song, Y. G. Anissimov, J. Zhao, A. V. Nechaev, A. Nadort, D. Jin, T. W. Prow, M. S. Roberts, and A. V. Zvyagin, "Background free imaging of upconversion nanoparticle distribution in human skin," *J. Biomed. Opt.* **18**, 061215-061215 (2013).
13. S. A. Hilderbrand and R. Weissleder, "Near-infrared fluorescence: application to *in vivo* molecular imaging," *Curr. Opin. Chem. Biol.* **14**, 71-79 (2010).
14. U. Resch-Genger, M. Grabolle, S. Cavaliere-Jaricot, R. Nitschke, and T. Nann, "Quantum dots versus organic dyes as fluorescent labels," *Nat. Meth.* **5**, 763-775 (2008).
15. W. Denk, J. H. Strickler, and W. W. Webb, "Two-photon laser scanning fluorescence microscopy," *Science* **248**, 73-76 (1990).
16. C. Buehler, K. H. Kim, C. Y. Dong, B. R. Masters, and P. T. So, "Innovations in two-photon deep tissue microscopy," *Engineering in Medicine and Biology Magazine, IEEE* **18**, 23-30 (1999).
17. F. Auzel, "Upconversion and anti-stokes processes with f and d ions in solids," *Chem. Rev.* **104**, 139-174 (2004).
18. J. Hecht, "Short history of laser development," *Optical Engineering* **49**, 091002-091002-091023 (2010).
19. S. Heer, K. Kömpe, H. U. Güdel, and M. Haase, "Highly Efficient Multicolour Upconversion Emission in Transparent Colloids of Lanthanide-Doped NaYF<sub>4</sub> Nanocrystals," *Adv. Mater.* **16**, 2102-2105 (2004).
20. S. Heer, O. Lehmann, M. Haase, and H. U. Güdel, "Blue, Green, and Red Upconversion Emission from Lanthanide-Doped LuPO<sub>4</sub> and YbPO<sub>4</sub> Nanocrystals in a Transparent Colloidal Solution," *Angewandte Chemie International Edition* **42**, 3179-3182 (2003).
21. G. Chen, H. Qiu, P. N. Prasad, and X. Chen, "Upconversion Nanoparticles: Design, Nanochemistry, and Applications in Theranostics," *Chem. Rev.* (2014).
22. G. Chen, G. Somesfalean, Y. Liu, Z. Zhang, Q. Sun, and F. Wang, "Upconversion mechanism for two-color emission in rare-earth-ion-doped Zr O<sub>2</sub> nanocrystals," *Physical Review B* **75**, 195204 (2007).
23. M. P. Hehlen, G. Frei, and H. U. Güdel, "Dynamics of infrared-to-visible upconversion in Cs<sub>3</sub>Lu<sub>2</sub>Br<sub>9</sub>: 1% Er<sup>3+</sup>," *Physical Review B* **50**, 16264 (1994).
24. J. Suyver, A. Aebischer, D. Biner, P. Gerner, J. Grimm, S. Heer, K. Krämer, C. Reinhard, and H. Güdel, "Novel materials doped with trivalent lanthanides and transition metal ions showing

- near-infrared to visible photon upconversion," *Optical Materials* **27**, 1111-1130 (2005).
25. K. W. Krämer, D. Biner, G. Frei, H. U. Güdel, M. P. Hehlen, and S. R. Lüthi, "Hexagonal sodium yttrium fluoride based green and blue emitting upconversion phosphors," *Chem. Mater.* **16**, 1244-1251 (2004).
  26. M. Pollnau, D. Gamelin, S. Lüthi, H. Güdel, and M. Hehlen, "Power dependence of upconversion luminescence in lanthanide and transition-metal-ion systems," *Physical Review B* **61**, 3337 (2000).
  27. Y. Wang, S. Smolarek, X. Kong, W. J. Buma, A. M. Brouwer, and H. Zhang, "Effect of surface related organic vibrational modes in luminescent upconversion dynamics of rare earth ions doped nanoparticles," *J. Nanosci. Nanotechnol.* **10**, 7149-7153 (2010).
  28. J.-C. Boyer and F. C. Van Veggel, "Absolute quantum yield measurements of colloidal NaYF<sub>4</sub>: Er<sup>3+</sup>, Yb<sup>3+</sup> upconverting nanoparticles," *Nanoscale* **2**, 1417-1419 (2010).
  29. F. Wang, J. Wang, and X. Liu, "Direct Evidence of a Surface Quenching Effect on Size-Dependent Luminescence of Upconversion Nanoparticles," *Angew. Chem.* **122**, 7618-7622 (2010).
  30. J.-C. Boyer, M.-P. Manseau, J. I. Murray, and F. C. van Veggel, "Surface modification of upconverting NaYF<sub>4</sub> nanoparticles with PEG-phosphate ligands for NIR (800 nm) biolabeling within the biological window," *Langmuir* **26**, 1157-1164 (2009).
  31. R. Gref, M. Lück, P. Quellec, M. Marchand, E. Dellacherie, S. Harnisch, T. Blunk, and R. Müller, "'Stealth'corona-core nanoparticles surface modified by polyethylene glycol (PEG): influences of the corona (PEG chain length and surface density) and of the core composition on phagocytic uptake and plasma protein adsorption," *Colloids and Surfaces B: Biointerfaces* **18**, 301-313 (2000).
  32. R. S. Niedbala, H. Feindt, K. Kardos, T. Vail, J. Burton, B. Bielska, S. Li, D. Milunic, P. Bourdelle, and R. Vallejo, "Detection of analytes by immunoassay using up-converting phosphor technology," *Anal. Biochem.* **293**, 22-30 (2001).
  33. T. Pellegrino, L. Manna, S. Kudera, T. Liedl, D. Koktysh, A. L. Rogach, S. Keller, J. Rädler, G. Natile, and W. J. Parak, "Hydrophobic nanocrystals coated with an amphiphilic polymer shell: a general route to water soluble nanocrystals," *Nano Lett.* **4**, 703-707 (2004).
  34. K. Liu, J. A. Holz, Y. Ding, X. Liu, Y. Zhang, T. Langping, X. Kong, B. Priem, A. Nadort, S. A. G. Lambrechts, M. C. G. Aalders, W. J. Buma, P. D. Y. Liu, and H. Zhang, "Targeted labeling of early-stage tumor spheroid in chorioallantoic membrane model with upconversion nanoparticles," *Nanoscale* (2014).
  35. V. K. Sreenivasan, A. V. Zvyagin, and E. M. Goldys, "Luminescent nanoparticles and their applications in the life sciences," *J. Phys.: Condens. Matter* **25**, 194101 (2013).
  36. A. E. Guller, A. N. Generalova, E. V. Petersen, A. V. Nechaev, I. A. Trusova, N. N. Landyshev, A. Nadort, E. A. Grebenik, S. M. Deyev, A. B. Shekhter, and A. V. Zvyagin, "Cytotoxicity and non-specific cellular uptake of bare and surface-modified upconversion nanoparticles in human skin cells," *Nano Research* (in press) (2014).